Velichkova et al., http://www.jcb.org/cgi/content/full/jcb.200911020/DC1

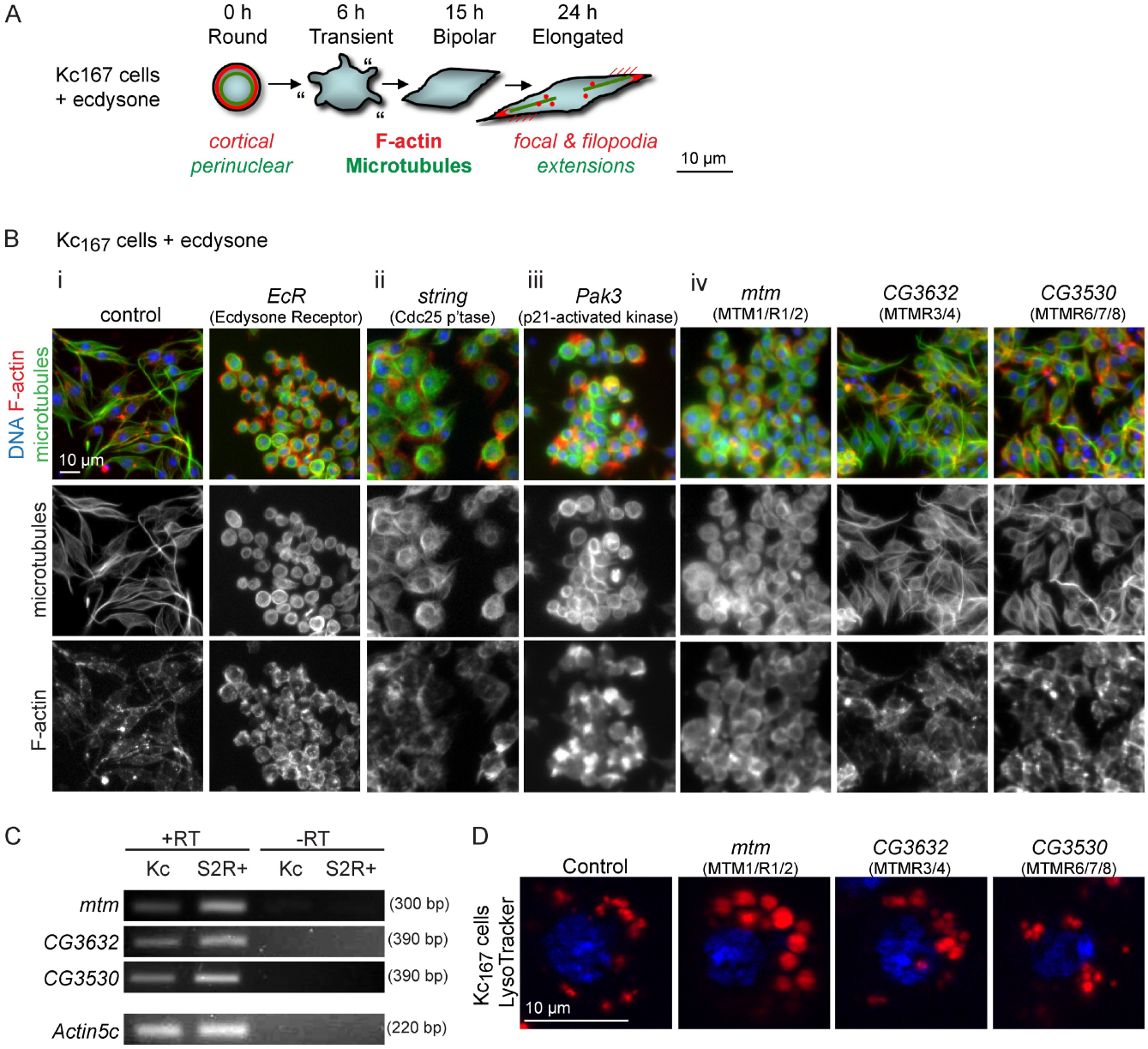

Figure S1. **RNAi screen for Kc_{167} cell shape change.** (A) Kc_{167} cell response to ecdysone, highlighting cytoskeletal remodeling that coincides with cell shape change. (B, i–iv) Examples of results acquired in kinase phosphatase RNAi screen of ecdysone-treated Kc_{167} cells stained for DNA (blue), microtubules (green), and F-actin (red); single channel is shown below. (i) Control wells. Cells without dsRNA elongated after ecdysone addition. *EcR* dsRNA to disrupt ecdysone reception inhibited the response, and cells remained round. (ii) Effects of known G2/M cell cycle regulators. *string* RNAi resulted in enlarged cells with shorter protrusions. (iii) Effects of F-actin regulators. *Pak3* RNAi resulted in a lack of microtubule protrusions and polarized distribution of F-actin. (iv) MTM phosphatases. Of the three fly homologues (*mtm*, *CG3632*, and *CG3530*) for active MTM phosphatases, only *mtm* RNAi resulted in round cells. The *mtm* gene encodes the single *Drosophila* orthologue of the human MTMR2/MTM1/MTMR1 subfamily (53–66% identity) with the highest homology to human than to other fly-encoded MTMs (36–40% identity). (C) MTM active phosphatases are coexpressed in two different hemocyte cell culture lines, Kc_{167} and $S2R^+$ cells. (D) Of the three active MTM homologues, only *mtm* RNAi resulted in dramatic increase in endolysosome size (red, LysoTracker; blue, DNA).

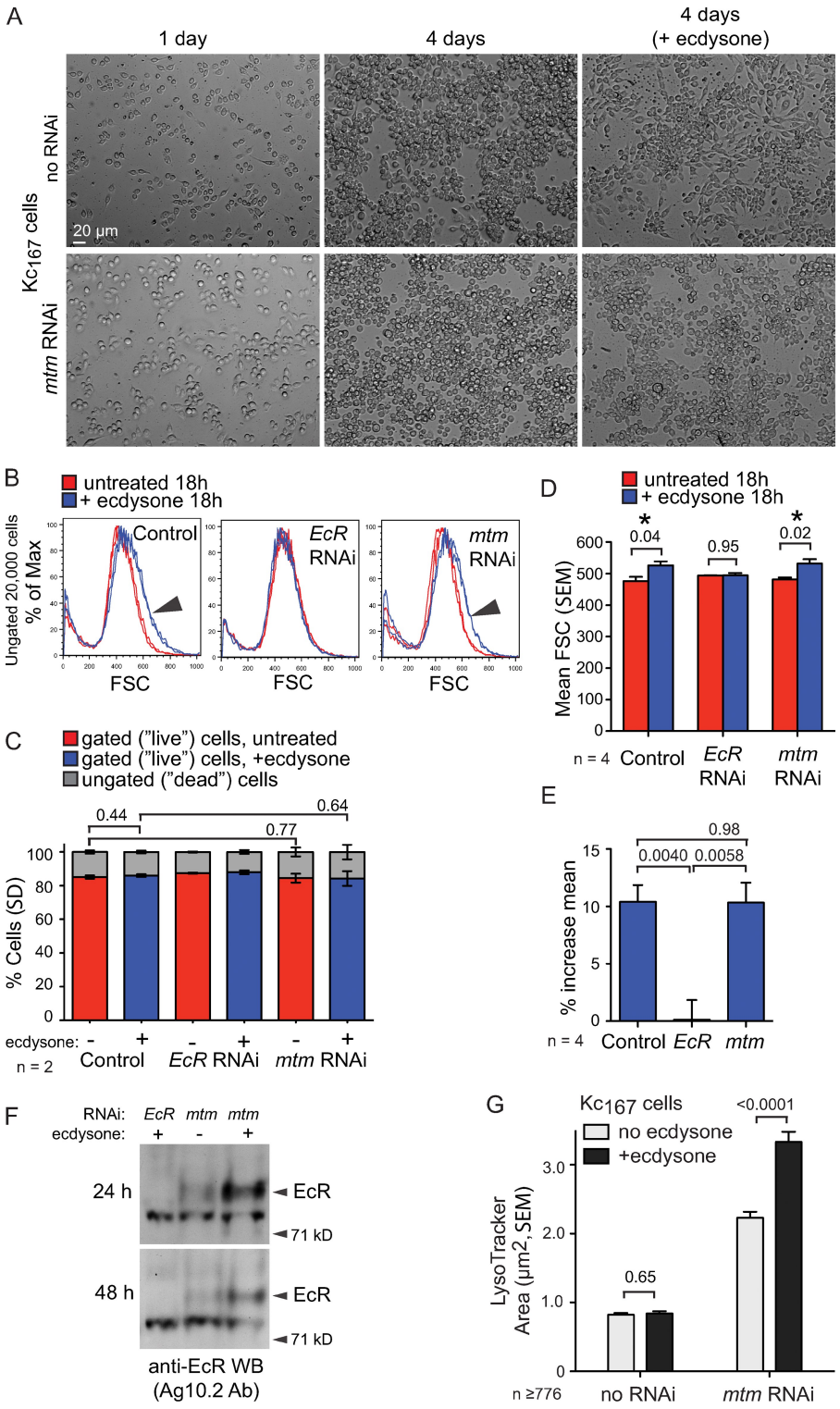

Figure S2. ***mtm* is not required for normal Kc$_{167}$ cell growth, viability, or ecdysone responses.** (A) Images depicting normal Kc$_{167}$ cell populations 1 and 4 d after *mtm* RNAi, including 1 d with ecdysone. Quantification shown in Fig. 1 D. (B) Flow cytometry of 20,000 ungated control (left) and *EcR* or *mtm* RNAi–treated Kc$_{167}$ cells (right) after 18 h mock (red) or ecdysone treatment (blue). Forward scatter (FSC) distributions shown for replicate samples from one representative experiment. An ecdysone-induced upward shift in FSC, indicative of increased cell size, seen in control and *mtm* RNAi cells (arrowheads) but not cells depleted for *EcR*. (C) Similar percentages of cells isolated in live cell gates determined from FSC/SSC plots for control and *mtm* RNAi cells both in absence (red) or presence (blue) of ecdysone. (D) Normal upward shift in the forward scatter upon ecdysone treatment of both control and *mtm* RNAi cells. No shift was seen with *EcR* RNAi. (E) Percent increase in the mean forward scatter distribution 18 h after ecdysone induction from results in D. (F) Ecdysone-induced up-regulation of EcR protein levels in *mtm* RNAi Kc$_{167}$ cells, detected by Western blotting (WB) 24 (top) and 48 h (bottom) after ecdysone (+). Western blots using anti-EcR Ag10.2 detects a band at a predicted molecular mass (top) that is absent with *EcR* RNAi. (G) Area of individual LysoTracker-positive compartments in *mtm* RNAi cells exhibited a further, ecdysone-responsive increase in size. Error bars indicate SEM.

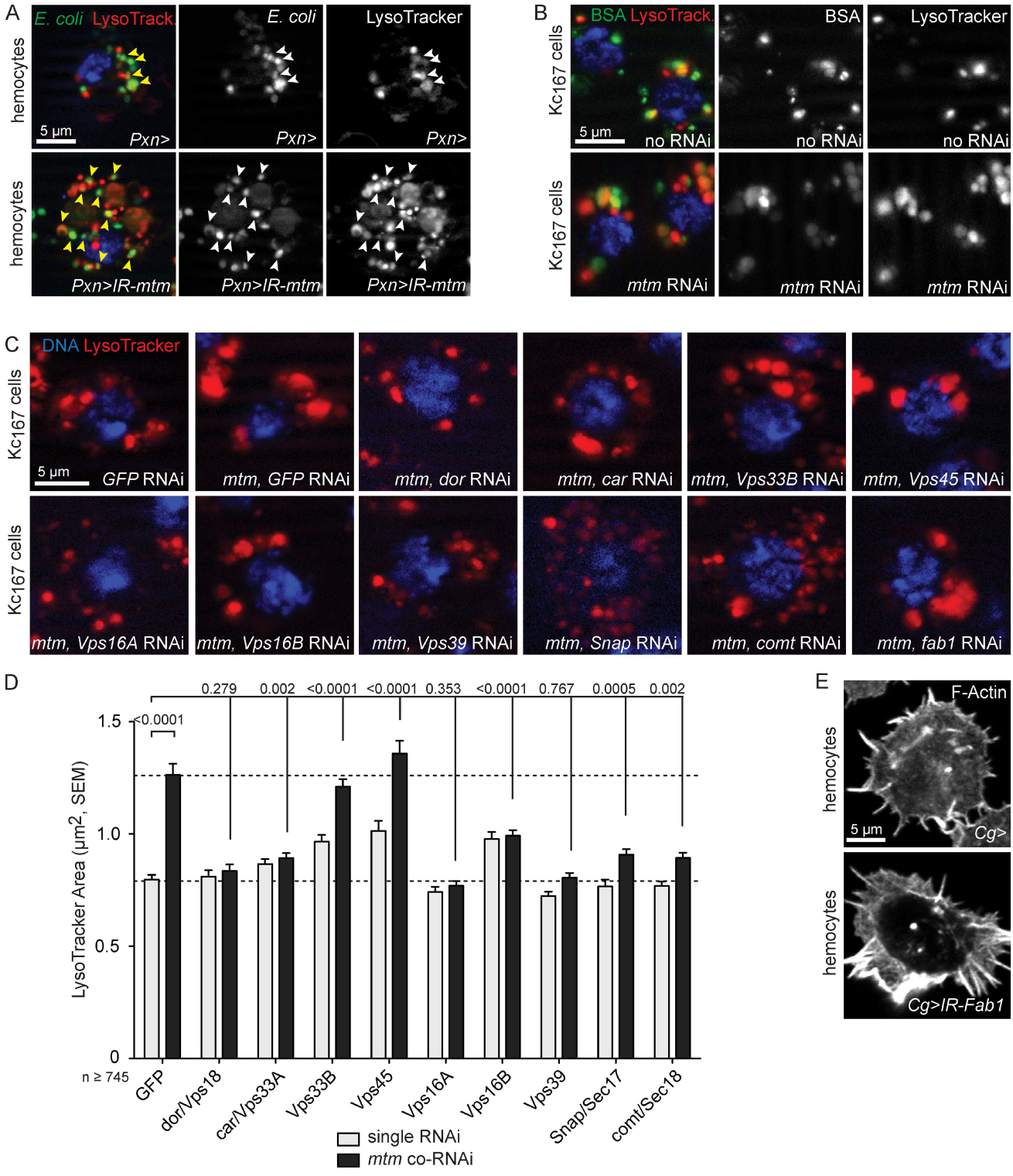

Figure S3. **Mtm-dependent defects depend on HOPS complex but not Fab1 kinase.** (A) Engulfment of *E. coli* (green) and delivery to LysoTracker endolysosomes (red) observed in control and *mtm*-depleted hemocytes (yellow arrowheads). White arrowheads, single channel. (B) BSA-488 (green) uptake and delivery to LysoTracker-positive organelles (red) in control and *mtm* RNAi Kc_{167} cells. (C and D) Miniscreen of endolysosome size in single- and *mtm* coRNAi–treated Kc_{167} cells identified suppressors of *mtm*-enlarged endolysosomes. (C) LysoTracker organelles (red) in Kc_{167} cells with coRNAi for genes encoding components of HOPS complex, SNAREs, and *fab1*. (D) Quantification of mean endolysosomal area as in Fig. 5. *mtm* RNAi–enlarged endolysosomes suppressed by codepletion of HOPS components *dor/Vps18, Vps16A*, or *Vps39* (no significant difference in size compared with *GFP* RNAi control) and partially suppressed with *car/Vps33A, Snap/Sec17*, or *comt/Sec18* (mean size reduced but statistically still different from WT control). Suppression seen with only one of three Sec1/Munc18 homologues (*car/Vps33A* but not *Vps33B* or *Vps45*) and one of two *Vps16* homologues (*Vps16A* but not *Vps16B*). (E) *Fab1* RNAi does not disrupt hemocyte cell spreading or protrusion formation. Error bars indicate SEM.

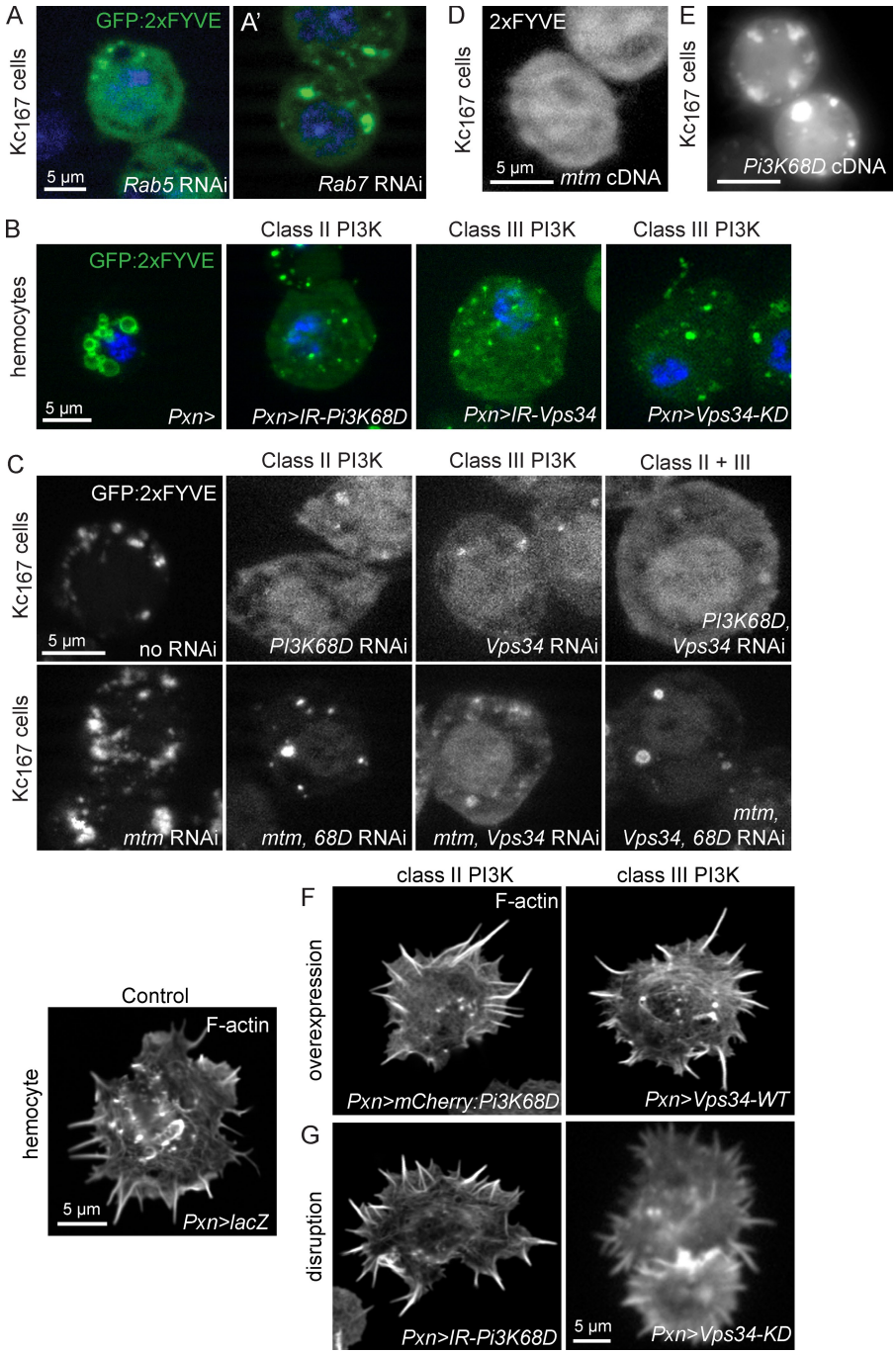

Figure S4. **Both class II and III Pi3Ks required for PI(3)P accumulation.** PI(3)P distribution and accumulation as detected by GFP:2xFYVE. (A) In Kc_{167} cells, GFP:2xFYVE became mostly diffuse in the cytoplasm with *Rab5* RNAi, indicative of loss of localized PI(3)P. (A') Partial or unsubstantial effect on PI(3)P was observed upon *Rab7* RNAi. (B) Pxn-GAL4 hemocyte-driven GFP:2xFYVE was detected as rings in WT cells and became similarly diffuse with few remaining puncta upon either *IR-Pi3K68D*, *IR-Vps34*, or expression of *Vps34-KD*, as seen using Cg-GAL4 in Fig. 7. (C) In Kc_{167} cells, PI(3)P distribution detected upon *Pi3K68D* and *Vps34* single and combined *mtm* RNAi conditions. Quantification shown in Fig. 5 C. (D) Expression of WT *mtm* cDNA resulted in PI(3)P turnover, as detected by diffuse GFP:2xFYVE in Kc_{167} cells (top). (E) Expression of WT *Pi3K68D* cDNA led to an accumulation of PI(3)P, as detected by expanded compartments and increased brightness of localized GFP:2xFYVE. (F and G) Primary hemocytes stained for F-actin. Normal hemocyte spreading and cell protrusions upon *Pxn-GAL4* targeted class II or III Pi3K functions with overexpression of *mCherry:Pi3K68D* (F) or *Vps34-WT* or disruption by *IR-Pi3K68D* or *Vps34-KD* (G).

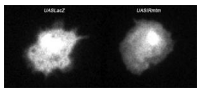

Video 1. **Mtm alters cell protrusion formation and dynamics.** Time-lapse fluorescence microscopy video of cortical dynamics in live control and *mtm*-depleted GFP-positive hemocytes (Pxn-GAL4) taken with a fluorescent spinning-disk confocal microscope (DSU). Arrowheads indicate examples of protrusions observed to extend/retract perpendicular to the cell surface in control cells (left) versus short protrusions seen to move radially along the cell periphery in *mtm*-depleted hemocytes (right). Frame rates were taken every 10 s for 5 min.

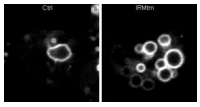

Video 2. **Mtm alters PI(3)P compartment dynamics.** Time-lapse confocal microscopy video of PI(3)P detected with mCherry2x-FYVE in live control (ctrl) and *mtm*-depleted hemocytes (Cg-GAL4) taken with a point-scanning confocal microscope (FV1000). Note that extension and retraction of apparent tubulation from compartments in control cells (left) were not observed in *mtm*-depleted cells (right). Frames were taken every 15 s for 5 min.

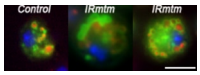

Video 3. **Tubulation from GFP:Rab7 compartments.** Time-lapse microscopy video of GFP:Rab7 and LysoTracker organelles in live control and *mtm*-depleted hemocytes (Pxn-GAL4) taken with a spinning-disk microscope (DSU). Note the apparent tubulation from GFP:Rab7 compartments near the end of the video in control cells (left), which is undetected in *mtm*-depleted cells (middle and right). Frames were taken every 10 s for 10 min. Bar, 10 μm.

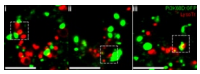

Video 4. **Dynamic association of motile Pi3K68D:GFP with endolysosomes.** Time-lapse confocal microscopy video of Pi3K68D:GFP and LysoTracker in live hemocytes (Pxn-GAL4) taken with a point-scanning confocal microscope (FV1000). Three representative cells are shown. Note the motility and association of Pi3K68D:GFP with periphery of LysoTracker-containing organelles. Frames were taken every 15 s for 5 min. Bar, 5 μm.

Table S1. ***mtm* has essential roles in hemocytes and muscle, substitutable with human *MTMR2* and antagonistic to *Pi3K68D***

Tissue	Construct	Phenotype[a]	*mtm:GFP*	*GFP:MTMR2*	*IR-Pi3K68D*	*Vps34-KD*[b]
Ectopic; *Act5c-GAL4*	*IR-mtm*	Lethal; early pupal	Viable	Viable	Lethal; eclosion	Lethal; early pupal
Hemocytes, fat body; *Cg-GAL4*	*IR-mtm*	Lethal; pharate	Viable	Viable	Lethal; eclosion	Lethal; eclosion
Cg-GAL4	*Pi3K68D:GFP*	Semilethal; pharate	ND	ND	ND	ND
Cg-GAL4	*Vps34-WT*	Viable	ND	ND	ND	ND
Hemocytes; *Pxn-GAL4*	*IR-mtm*	Semilethal; eclosion	Viable	Viable	Semilethal; adults	Lethal; eclosion
Pxn-GAL4	*Pi3K68D:GFP*	Viable	ND	ND	ND	ND
Pxn-GAL4	*Vps34-WT*	Viable	ND	ND	ND	ND
Muscle[c]; *24B-GAL4*	*IR-mtm*	Lethal; pharate	Viable	Viable	Viable	Lethal; pharate
Muscle; *DMef2-GAL4*	*IR-mtm*	Semilethal; eclosion	Viable	Viable	Viable	Semilethal; eclosion
DMef2-GAL4	*Pi3K68D:GFP*	Lethal; larval	ND	ND	ND	ND
Ectoderm, epidermis; *69B-GAL4*	*IR-mtm*	Lethal; late pupal	Viable	Viable	Viable	Lethal; early pupal
Epidermis; *ptc-GAL4*	*IR-mtm*	Misoriented bristles	Normal bristles	Normal bristles	Normal bristles	ND

GAL4 lines tested with I*R-mtm* resulting in no visible phenotype include: *en-GAL4*, *arm-GAL4* (epidermis); *ey-GAL4*, *GMR-GAL4* (eye); *Lsp2-GAL4* (fat body); and *elav-GAL4*, *nrv-GAL4* (nervous system). Results are shown for lethal and visible phenotypes detected with GAL4-driven expression of RNAi or cDNAs targeted to specific tissues, and genetic interactions tested between *IR-mtm* with either WT *mtm* cDNA or human *MTMR2* cDNA, *IR-Pi3K68D* RNAi, or *Vps34-KD* kinase-dead cDNA, and viability with expression of WT *Pi3K68D* or *Vps34* cDNAs. GAL4/UAS crosses were tested at 29°C. Viable results from crosses were not shown between *Act5c-GAL4* with *IR-Pi3K68D*; *Cg-GAL4* with *IR-Pi3K68D*, *Vps34-KD*, *mtm* cDNA, or *Vps34* cDNA; *Pxn-GAL4* with *IR-Pi3K68D*; *24B-GAL4* with *IR-Pi3K68D* or *Vps34-KD*; DMef2-GAL4 with *IR-Pi3K68D* or *Vps34-KD*; *69B-GAL4* with *IR-Pi3K68D*; and similar lethal and rescue results with *IR-mtm* expression in hemocytes with hmlΔ-GAL4.

[a]Lethality with UAS-driven expression of RNAi inverted repeat (IR) or cDNAs, as shown. Genotypes included *UAS-GFP* to mimic conditions with two UAS- constructs, as in subsequent columns testing rescue and genetic interactions.

[b]cDNA-carrying kinase-dead mutation.

[c]May be expressed in other additional tissues.